2008

Mechanization of a High Aspect Ratio Wing for Aerodynamic Control

Geoffrey J. Frank

James J. Joo

Brian Sanders

David M. Garner

Andrew P. Murray

Mechanization of a High Aspect Ratio Wing for Aerodynamic Control†

GEOFFREY J. FRANK,[1,*] JAMES J. JOO,[1] BRIAN SANDERS,[2] DAVID M. GARNER[3] AND ANDREW P. MURRAY[1]

[1]*University of Dayton, Dayton, Ohio 45469, USA*

[2]*Air Combat Command, Langley AFB, Langley, VA 23665, USA*

[3]*Air Vehicles Directorate, Air Force Research Laboratory, Wright-Patterson AFB, OH 45433, USA*

ABSTRACT: Investigations are conducted to mechanize a controlled spanwise-varying airfoil camber change for a high aspect ratio wing, resulting in optimized aerodynamic performance for a aircraft that changes weight by 50% over its mission. Mechanisms to achieve these shape changes are designed based on two separate design methodologies: a rigid body kinematics approach and a compliant mechanism approach. A framework for optimizing mechanisms based on each approach is presented. Differences between the approaches are illustrated through the design of a mechanism for a specific set of airfoil shapes. Mechanisms are evaluated based on the error in the shapes and on the energy efficiency of the systems.

Key Words: morphing aircraft, mechanism design, compliant mechanism, adaptive wing, sensorcraft.

INTRODUCTION

THE United States Air Force has great interest in developing advanced Intelligence, Surveillance, and Reconnaissance (ISR) platforms. It is envisioned that the capabilities of these vehicles will dramatically surpass the capabilities of existing ISR platforms in both time on station and information gathering capability. In the forefront of this effort is research toward a next generation high altitude long endurance sensor platform, which has been designated Sensorcraft. When the Sensorcraft becomes operational it will feature antenna arrays that are structurally embedded and integrated into the wings and fuselage of the vehicle. These sensors will enable a continuous 360° coverage using state-of-the-art radar and standoff capability. In addition, the Sensorcraft will fly at higher altitudes and have longer loiter times over the target area than are currently possible. Overall it is expected to command significantly greater mission effectiveness than current manned or unmanned ISR platforms.

Although, the exact configuration of the Sensorcraft has not been determined, a few planforms have been suggested to meet the demanding performance needs. One design that is being investigated is the joined-wing configuration shown in Figure 1. Reich et al. (2004) discussed the aerodynamic performance of this vehicle for cruise, loiter, and other critical mission segments. They proposed some scenarios to actively control the aerodynamic performance. Perhaps the most promising scenario is large area, distributed control using leading edge and trailing edge control surfaces. With such a system the wing would be able to reconfigure itself through the continuous deformation of the structure to optimize its geometry to suite the current altitude, airspeed, and lift-to-drag (L/D) ratio requirements. Compared to current aircraft this would enable either a reduction in gross weight for fixed endurance or an increase in endurance for fixed gross weight.

Reich et al. (2004) identified airfoil shapes to maximize L/D in cruise. Because nearly half the takeoff weight for the Sensorcraft is fuel, significantly different performance conditions exist during a typical mission. They showed that the majority of the aerodynamic improvement could be achieved by deflecting a smooth trailing edge control surface with the capability to vary its deflection along the span. The purpose of this study is to investigate structurally integrated mechanisms to enable this continuous camber change.

BACKGROUND

Some attempts to create smoothly varying surfaces have previously been pursued. The Mission Adaptive

†This article was originally presented at the Fifteenth International Conference on Adaptive Structures and Technologies (2004 ICAST).
*Author to whom correspondence should be addressed.
E-mail: geoffrey.frank@udri.udayton.edu

Wing (Hall, 1989) flight-tested a clever configuration of rigid mechanical linkages to smoothly deploy leading and trail edges. More recently, the Defense Advanced Research Projects Agency (DARPA) Smart Wing Project (Kudva, 2004) demonstrated an innovative configuration of ultrasonic motors, rotating bars, and flexible skins to create a system that can deform almost continuously along the span. Skelton (2001) has discussed other emerging techniques that might also enable this desired result. In this investigation we focus on methods to accomplish the desired shape changes using compliant mechanism based approaches. We investigate both lumped and distributed compliant mechanisms. Of course conventional hinged control surfaces are also an option, but the purpose of this study is to investigate newer approaches for actuator, structure, and mechanism integration.

Compliant mechanisms derive their name from the fact that they achieve mobility, at least in part, though compliance, i.e., elastic deformations of one or more of their links and joints, rather than exclusively through relative motion at the joints, as discussed in previous papers by Joo (2001). The category of compliant mechanism includes both multi-body mechanisms consisting of one or more joints and flexible links and single-body mechanisms without joints.

In this article, we investigate two different approaches to designing mechanisms: a rigid body kinematic design method and a compliant mechanism design method. In the remainder of this article the kinematic design is referred to as "lumped compliance" and the compliant mechanism design is referred to as "distributed compliance". A lumped compliant mechanism has a discrete number of flexural pivots (sometimes called living hinges) that emulate the function of a conventional hinge joint by concentrating flexion to a few regions. Due to the characteristic of this mechanism, some conventional rigid body mechanisms can be converted directly into lumped compliant mechanisms by replacing revolute hinges with living hinges without an additional synthesis process.

When the flexure of the mechanism is not concentrated at a few discrete locations, the mechanism is labeled as a distributed compliant mechanism. Distributed compliant mechanisms may offer superior reliability compared to lumped compliant mechanisms because the flexion is not concentrated in a few regions and stress concentrations are avoided. However, energy requirements may increase relative to a lumped compliant mechanism since, in general, energy may be required to deform the mechanism in addition to the energy required to react external loads. In distributed compliant mechanisms, it is the topology, shape, and size of the material continuum that give these mechanisms motion and the force transmission capability.

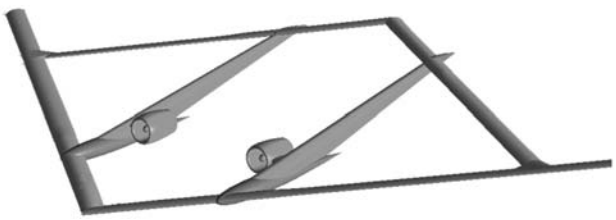

Figure 1. *Sensorcraft concept vehicle.*

In the following sections methods for mechanism design are developed and applied to the problem of producing a smoothly varying camber change for the control of a high altitude wing. Basic design methods for each type of mechanism are described. To illustrate the design methods, a mechanism is designed using each approach for a specific set of airfoil shapes. Comparisons between the resulting distributed and lumped compliant mechanisms are made based on the discrepancy between the desired and achieved airfoil shapes and based on the actuator work required to move the mechanisms through the range of motion required for the airfoil.

DESIGN METHODS

This section describes the fundamental elements used to design compliant mechanisms to enable an adaptively shaped airfoil. We utilize two different design approaches: lumped compliance and distributed compliance. Each technique has common goals: minimize shape error, limit actuator loads, identify locations of actuators, and address issues associated with structural design, such as material integration. A common requirement in each design method is that the outer moldline of the airfoil have a constant arclength during the deformation. This requirement arises from a desire to minimize the work expended in deforming the airfoil surface.

Lumped Compliance

Our process for designing lumped compliant mechanisms uses methods developed for studying the statics and kinematics of rigid bodies. The initial portion of the design process assumes the airfoil can be approximated as a set of infinitely rigid bodies linked by joints of negligible stiffness. In later stages of the design, the potential for flexible members and joints of finite stiffness is incorporated into the design. Joints of finite stiffness connecting relatively rigid sections result in a lumped compliant structure that, in some cases, may be similar to structures developed from a distributed compliant mechanism approach.

The problem of designing a lumped compliant mechanism that can meet an arbitrary number of profiles may be specified as: "given a set of specific

outer profiles, can a mechanism be synthesized that meets a set of target profiles within a specific tolerance while limiting actuator loads to an achievable level.'' The design begins with a specified set of outer surface profiles, specified based on aerodynamic performance criteria (i.e., airfoil shapes). To permit a mechanism to be developed, all profiles must have equal arclength. These profiles may be specified by discreet points or by functions. For this process, the profiles are interpolated at a set of M equally spaced locations.

The process begins by identifying rigid bodies that represent the longest segments of the outer skin that can move through all of a set of L defined profiles within some predefined tolerance, δ. We take n sequential points on each profile and find the rigid body motion that optimally moves a rigid body into each profile. This similarity transform is a variation on the so-called *image registration problem*, for which various solutions have been determined (Arun, 1987); (Horn, 1987); (Umeyama, 1991). The solution defined here is one that, though restricted to two dimensional problems, has a closed form solution that always produces a rotation matrix.

The criterion used for finding the segments is stated as (with no implicit summation):

Given $\bar{x}_i$ ($i=1$, n) initial point locations in space and $\bar{\varepsilon}_{ij}$ ($i=1$, n) locations on the ($j=1$, L) profiles that we want to approximate, find θ_j and $\bar{d}_j (j=1,\ L)$ that minimize:

$$E = \sum_{i=1}^{n} \left[\underline{A}_j \bar{x}_i + \bar{d}_j - \bar{\varepsilon}_{ij}\right]^2 \tag{1}$$

$$\underline{A}_j = \begin{bmatrix} \cos(\theta_j) & -\sin(\theta_j) \\ \sin(\theta_j) & \cos(\theta_j) \end{bmatrix}$$

$$\bar{d}_j^T = \left[d_x, d_y\right]_j$$

Minimization of (1) is accomplished by solving:

$$\underline{A}_j \sum_{i=1}^{n} \bar{x}_i + n\bar{d}_j - \sum_{i=1}^{n} \bar{\varepsilon}_{ij} = 0 \tag{2a}$$

$$\bar{d}_j^T \underline{A}_j \underline{\hat{I}} \sum_{i=1}^{n} \bar{x}_i - \sum_{i=1}^{n} \left(\bar{\varepsilon}_{ij}^T \underline{A}_j \underline{\hat{I}} \bar{x}_{ij}\right) = 0 \tag{2b}$$

$$\underline{\hat{I}} = \begin{bmatrix} 0 & -1 \\ 1 & 0 \end{bmatrix}$$

Equations (2) form a set of three simultaneous equations, which can be re-arranged to provide an explicit solution for θ_j, d_{xj}, and d_{yj}.

Identification of the surface segments that meet the design tolerance when moved as rigid bodies is a two-step process. First, $\bar{x}_i$ is populated by data taken from a segment of any one of the L surface profiles, say, Profile 1. Equations (2) are used to determine the rigid body transformation that most closely aligns equal arclength segments of each of the other $L-1$ profiles with the segment from Profile 1. An average segment shape is then formed from the point-by-point average of the locations of the points on the transformed profiles. This average profile forms a best approximation to the error-minimizing segment shape and is assigned to $\bar{x}_i$ in place of the original estimate. Equations (2) are then used a second time to find the transformations that most closely bring the new estimate of $\bar{x}_i$ into alignment with the L segment profiles. The maximum error for the segment is checked on a point-by-point basis:

$$E_{\max} = \max\left\{\left|\bar{\varepsilon}_{ij} - \bar{x}_i\right|\right\} i = 1, n; \quad j = 1, L \tag{3}$$

The length of the segment (or number of points n) is adjusted until $E_{\max} < \delta$ for a specific segment. The process is repeated for segments around the perimeter of the skin. Alternate processes for identifying segment lengths are presented in Korte et al. (2006).

Motion of the segments that form the outer skin is controlled by links and actuators, which, for purposes of initial design, are treated as 2D members with pinned joints at the ends. One end of the link or actuator is attached to a point on the outer skin and the other end is connected to a point rigidly fixed in space. For a mechanism that forms a closed profile composed of N segments, we can generate a one degree-of-freedom (DOF) system using $(N-1)$ links and 1 actuator.

For design purposes, several potential locations for links and actuators may be selected on each skin segment. For each potential location for a linkage, the first end is selected as a point on a skin segment, where the specific location is selected based on mechanical considerations such as providing enough space for a joint under the skin surface. The second end of the linkage is defined as a point lying on the perpendicular bisector to a line through the locus of points of the first end's position when it is moved with the rigid body skin segment to which it is attached. Potential locations for actuators are defined such that the first end is on a skin segment and the second end lies on a line parallel (or nearly parallel) to the line of motion the first end when the first end is moved with the skin segment. While sufficient for identifying mechanisms that may achieve the desired motion, these criteria for the selection of linkage and actuator locations do not necessarily produce mechanisms that meet the desired motion tolerance. As illustrated in the examples section of this article, many of the possible locations for linkages will results in mechanisms that have a larger position error than is desired. However, a sufficient number of potential mechanisms are identified with this method that one or more of the potential mechanisms will likely fall within the desired position tolerance.

The best locations for links and actuators are determined as points that minimize the overall forces

and provide the best approximation to the desired motion. For a configuration of N surface segments with Q possible actuator or linkage locations per segment and limiting the design to not more than one rigid link per skin segment, there are on the order of $Q^N N^2$ possible combinations. The possibility for a large number of potential mechanisms necessitates a method for ranking the options. For this design process the equations of statics are solved for each potential mechanism in the most-highly loaded position(s). Ranking of the potential mechanisms is performed as a weighted minimization of the sum of the forces in the actuators, linkages, and surface pieces, subject to the constraint that the actuator forces not exceed the capabilities of a realizable actuator.

To this point the design has not been assembled into a mechanism. The final step in the 2D design process is to utilize kinematics software to assemble the best options into a mechanism and identify those mechanisms that have the least overall position error. Approximations made in the preceding parts of the lumped mechanism design may lead to some solutions that do not meet the design target once it is assembled as a mechanism, but generally some configurations generated by this process will be capable of operation as mechanisms within the desired position tolerance.

Distributed Compliance

The topology design of distributed compliant mechanisms is developed by coupling the known synthesis process for topology design of a distributed compliant mechanism, as described by Ananthasuresh and Kota (1995), with an energy-based optimization problem. The goal of the design is to maximize the energy efficiency of the mechanized system while matching the airfoil's shape to the target desired shape as closely as possible. Since we have more than one goal to achieve, a multiple-criteria optimization is adopted. The objective function $F(A)$ is written as a linear combination of the terms involving shape error, input energy, and output energy, resulting in an objective function defined as:

$$\begin{aligned}\text{Minimize}\quad F(A) &= \omega_1(\text{Shape error}) - \omega_2(\text{Energy out}) \\ &\quad + \omega_3(\text{Energy in}) \\ &= \omega_1 \|X - X_o\| - \omega_2 \sum_{i=1}^{N_{\text{out}}} E_i^{\text{out}} + \omega_3 \sum_{i=1}^{N_{\text{in}}} E_i^{\text{in}}\end{aligned} \tag{4}$$

Subject to:

$$\begin{aligned} V &\le V^* \\ \delta_i &\le \delta^* (\text{or } \delta_i \ge \delta^*) \\ \omega_1 + \omega_2 + \omega_3 &= 1 \end{aligned}$$

where V is the mechanism volume, δ is the input displacement, ω_i are weighting functions, and starred quantities are prescribed values.

The first term on the right hand side of Equation (4) is a measure of the shape change error, where X is the location of the deformed curve and X_o is the location of the target curve. This term is the square of the difference between the original curve and the target. Using the square of the position error does not allow sign of the difference between positions of the two curves to be determined. The inability to determine the sign of the position error may present difficulties for applications where different levels of error must be required on opposite sides of the desired position curve, but, for most real applications, the sign of the discrepancy is not significant as long as the error is within some specified tolerance.

The next two terms in Equation (4) relate to the amount of actuator work required to deform the structure and to the amount of work that can be extracted from the air stream. The useful work (output energy in Equation (4)) of an adaptive structure is defined as the product of the deflection of the actuator tip and the load applied in the direction opposite of the deflection of the actuator tip. When the direction of load and deflection are the same, it is considered as work extracted from the air stream to deform the structure rather than as output energy.

The useful work is defined as:

$$\text{Useful work} = \sum_{i=1}^{N_{\text{out}}} E_i^{\text{out}} \tag{5}$$

where:

$$\begin{aligned} &\text{if } \text{sign}\left(\left(F_y^{\text{ex}}\right)_i\right) \ne \text{sign}(\Delta y_i), \quad E_i^{\text{out}} = -\left(F_y^{\text{ex}}\right)_i \Delta y_i \\ &\text{if } \text{sign}\left(\left(F_y^{\text{ex}}\right)_i\right) = \text{sign}(\Delta y_i), \quad E_i^{\text{out}} = 0 \end{aligned}$$

N_{out} is the number of nodes on the curve, F_y^{ex} is the external force in the y-direction, and Δy_i is the deformation in the y-direction under actuation and external load.

In the efficiency formulation derived by Joo et al. (2003), the actuator is assumed to be capable of achieving any input force up to some maximum value over the entire range of actuator motion. The same assumption is made here since the actuation force from some devices, such as hydraulic-actuators, is relatively constant over their operating range.

The input energy in (4) is related to the actuator force F_i as:

$$\text{Energy in} = \sum_{i=1}^{N_{\text{in}}} E_i^{\text{in}} = \sum_{i=1}^{N_{\text{in}}} F_i \cdot \delta_i \tag{6}$$

where N_{in} is the number of inputs and δ_i is the deflection at the actuator location. Note that δ_i is the deflection at the moving end of the actuator in the direction of the actuation force without any external load.

In this optimization technique the actuator location is selected at the beginning of the design process and the design variables are the cross section areas (A) of the frame elements. The topology optimization process distributes material to minimize the objective function with a given material. When the force is used as an input, it is possible that the optimal solution may be physically impractical, such as rigid body with no contact to a fixed boundary. To avoid this problem, either a displacement input (Joo et al., 2000) or an input constraint (Sigmund, 1997) may be specified. Here we use a displacement constraint. Also, for more than one target position problem, the optimization problem can be defined as:

$$\text{Minimize} \quad \sum_{j=1}^{n} (F(A))_j \quad (n = \text{number of target curve}) \tag{7}$$

The sensitivity of the energy output and input with respect to area is obtained from the direct derivative of the stiffness with respect to the cross sectional area of the frame elements:

$$\frac{\partial E_i^{\text{out}}}{\partial A} = \left(\frac{\partial K_i}{\partial A}\Delta y\right)\Delta y_i \tag{8}$$

$$\frac{\partial E_i^{\text{in}}}{\partial A} = -\left(\frac{\partial K_i}{\partial A}\delta\right)\delta_i \tag{9}$$

The sensitivity of the shape error term with respect to area is obtained using the chain rule:

$$\begin{aligned}&\frac{\partial}{\partial A}\left(\sqrt{(X - X_o)^2 + (Y - Y_o)^2}\right)\\ &= \frac{\partial}{\partial X}\left(\sqrt{(X - X_o)^2 + (Y - Y_o)^2}\right)\frac{\partial X}{\partial A}\\ &\quad + \frac{\partial}{\partial Y}\left(\sqrt{(X - X_o)^2 + (Y - Y_o)^2}\right)\frac{\partial Y}{\partial A}\end{aligned} \tag{10}$$

APPLICATION OF DESIGN PROCESSES

Using the general processes described above, mechanisms have been synthesized for a specific set of wing profiles related to one section of the Sensorcraft wing. Examples are shown for mechanisms using both distributed compliance and lumped compliance approaches.

Common to both the distributed and lumped compliance designs are a set of airfoil shapes and loads provided for the wing root of the Sensorcraft wing. These airfoil shapes have been generated with the objective of minimizing induced drag while requiring that the total lift coefficient equals the design lift coefficient and the total pitching moment coefficient equals zero (i.e., a trimmed vehicle). The airfoil shapes and associated surface pressures have been generated at a series of eight positions, covering the range of shapes required throughout the expected Sensorcraft mission. For all eight positions the airfoil surface maintains a constant arclength. Profiles for 'Position 1' (maximum airfoil camber) and 'Position 8' (minimum airfoil camber) are shown in Figure 2. In Figure 2, like in all illustrations throughout this article, the airfoils are shown as sections perpendicular to the wing's leading edge rather than as sections cut in a streamwise direction. The wing is swept back at 35°, resulting in a stream-wise airfoil of 21% thickness and a nominal chord of 2.02 m. Cross sections taken perpendicular to the wing's leading edge yield an airfoil of 25% thickness and a nominal chord of 1.64 m.

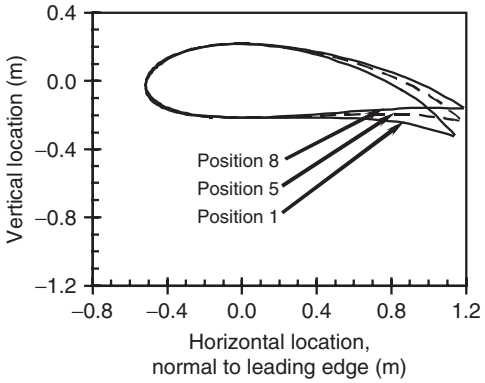

Figure 2. *Wing sections perpendicular to leading edge.*

Application for a Lumped Compliant Mechanism

DESIGN OF LUMPED COMPLIANT MECHANISM

The profiles shown in Figure 2 were broken into 500 equal arclength segments. Equations (2) and (3) were utilized to identify maximum lengths of segments that could move as rigid bodies and fall within ±6.35 mm of the target profiles for all positions. For this configuration, seven surface segments were required to meet the ±6.35 mm tolerance. These segments are shown in Figure 3(a).

Three points were defined on each of the seven skin segments as potential locations where rigid links could be used to control the motion of the skin segments. To provide space for hinges at the end of the links inside the skin, the points were chosen 25.4 mm inside the skin. Locations of the other end of each rigid link were

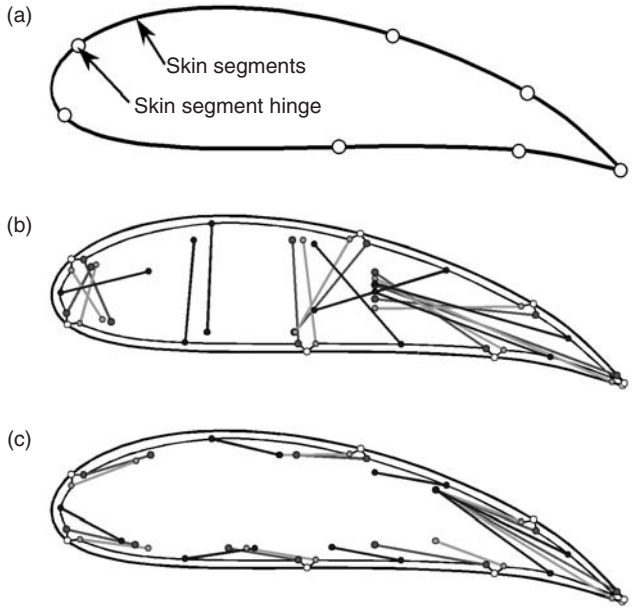

Figure 3. *Identification of components for lumped compliance mechanism (a) optimal hinge locations to align surface with eight specified profiles with $<\pm 6.35$ mm error (b) potential locations for rigid links for airfoil, and (c) potential locations for actuators for airfoil.*

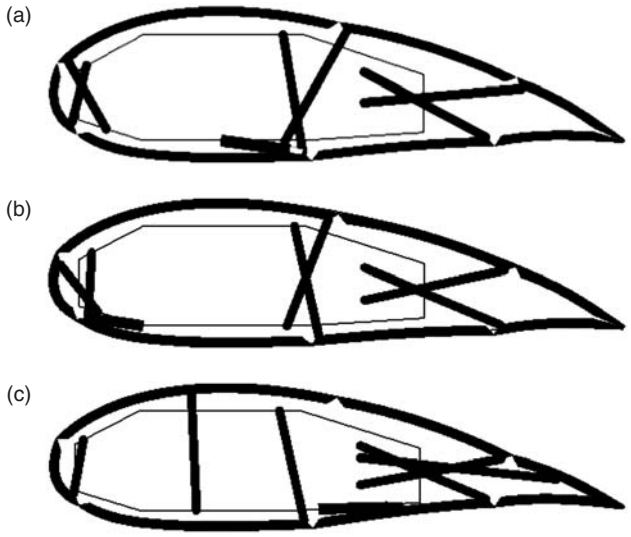

Figure 4. *Lumped compliance configurations selected after forming as a mechanism and moving to position of highest positional error: (a) option 1, (b) option 2, (c) option 3.*

defined from the intersection of the perpendicular bisector to the motion of the point on the skin for that hinge with the section that was not violated by any of the eight profiles. The 21 possible link locations are shown in Figure 3(b).

The same three points on each skin segment used for the rigid links were also used as potential hinge points for attaching an actuator. The other end of each potential actuator location was taken as a point closest to the direction of motion of the skin hinge point that also lay inside the area not violated by any of the eight profiles. The 21 possible actuator locations are shown in Figure 3(c).

To produce a one DOF mechanism with seven skin segments, it is necessary to have six rigid links and one actuator. The 21 potential link and actuator locations represent 107,163 possible configurations. For each configuration, a static solution for the forces in each member were computed based on the pressure distribution for the most highly loaded position (Position 1), assuming a 1.52 m span of wing. Based on the static solutions, potential configurations were eliminated that exceeded 4448 N actuation loads for the 1.52 m span. Configurations were also eliminated that had more than two rigid links in the middle of any skin segment, since these links generally do not provide accurate control of the surface positions. Solutions were selected that had low overall forces in the joints and links, by selecting configurations that had the lowest maximum magnitudes of force. The figure of merit (FOM) used for this selection was:

$$\text{Figure of Merit} = \sqrt{\left(F^2_{\text{max\_in\_joints}} + F^2_{\text{min\_in\_joints}} + F^2_{\text{max\_in\_links}} + F^2_{\text{min\_in\_links}}\right)} \tag{11}$$

Several configurations had a similar FOM. Their response as rigid mechanisms over their design range of motion was simulated using ProEngineer® software. Three of the mechanisms simulated using ProEngineer are shown in Figure 4. In Figure 4 they are moved to the position that produces the most error between the desired profile and the mechanism shape. Figure 4(c) shows that Option 3 diverges significantly from the desired shape. This error occurs because of approximations that are made in the early part of this design process, namely that the hinges in the skin segments are not required to remain connected and that the links are assumed to move on a circular arc, even though the points they are guiding may actually move on a complex path. However, despite these approximations, configurations can be found that meet the load and position requirements. For this design Option 1, shown in Figure 4(a), was selected for further evaluation.

To illustrate the 3D nature of the configuration, Figure 5 shows a 3D model of a single 1.52 m span section of the wing with the skin removed. The model shown includes a fuel tank and a truss used to represent an internal wing box that carries the majority of the bending and torsion loads for the structure.

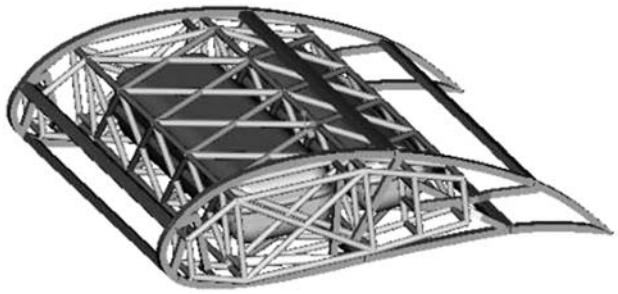

Figure 5. *Structure of lumped compliance mechanism wing with skin removed showing internal structures and possible fuel tank.*

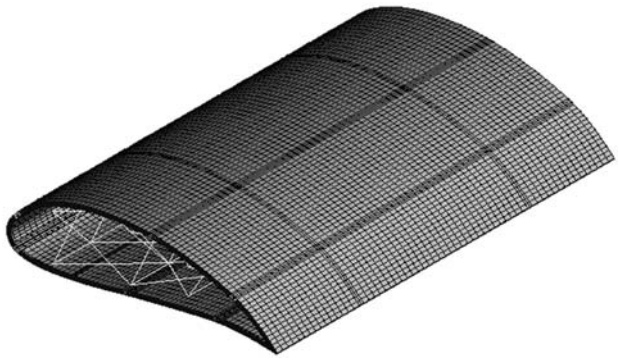

Figure 6. *Finite element analysis model used for optimizing the hinge stiffness for the lumped compliance system.*

IDENTIFICATION OF OPTIMAL HINGE STIFFNESS

The lumped compliance mechanism design process does not take into account the effects of finite stiffness hinges, which may be utilized to reduce loading on the actuators if selected properly. This section describes the process used to determine properties that could be used to design a controllable flexure hinge, using Shape Memory Polymers (SMP) for example, that would minimize actuator energy. The SMP composite in the hinge locations had to exhibit appropriate stiffness characteristics that would allow bending while minimizing translational displacements. To determine the material properties, some design criteria were defined: limit the actuator force range to $\pm 4448\,N$, minimize actuator energy, and limit the relative translation across any hinge to 0.254 mm in the x and y directions (where 'x' is perpendicular to the skin surface, 'z' is parallel to the hinge, and 'y' is perpendicular to the hinge in the plane of the skin).

For assessing the effect of different hinge properties, a finite element analysis (FEA) model of the mechanized wing section was developed and analyzed using HKS ABAQUS version 6.3.3. The model, shown in Figure 6, uses two-node beam elements for the actuator and for the internal structures that react loads from the actuator and linkages. Four-node shell elements are used for the internal linkages and wing skin panels. Linear spring elements are used at the hinge locations. The model is a 3.05 m wing section with clamped constraints applied to one end and a symmetry condition applied to the other end, thus representing a 6.10 m span, clamped at both ends. Quasi-static aerodynamic loads were applied based on the surface pressure distributions defined from a 2D aerodynamics code. Geometrically nonlinear analysis was used, although material properties were required to remain elastic.

Approximate relations for spring stiffness at the hinge locations were developed in terms of spring geometry and material moduli. Using these relationships, the stiffness of the hinges in the x, y, z, and rotational directions were calculated from extensional and shear moduli E and G, and spring length, width and thickness l, w, and t. The stiffness components, derived from beam and plate approximations, are calculated as:

$$\delta_x = \frac{Pw}{Elt} \Rightarrow K_x = \frac{Elt}{w} \quad \delta_y \approx \frac{Pw}{Glt} + \frac{Pw^3}{Elt^3} \Rightarrow K_y \approx \left(\frac{w}{Glt} + \frac{w^3}{Elt^3}\right)^{-1}$$

$$\delta_z \approx \frac{Pw}{Glt} \Rightarrow K_z \approx \frac{Glt}{w} \quad \theta_z \approx \frac{Mw}{El(t^3/12)} \Rightarrow K_{\theta z} \approx \frac{Elt^3}{12w} \qquad (12)$$

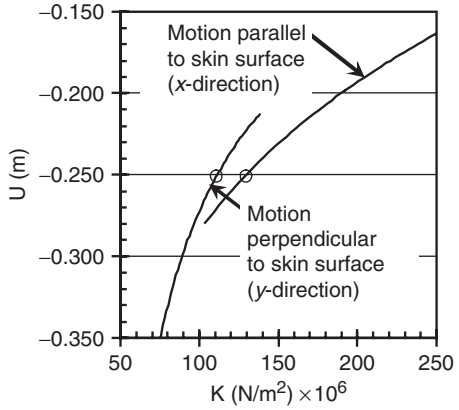

Figure 7. *Maximum relative motion between any two sections of skin at the hinges as a function of hinge translational stiffness for lumped compliance mechanism.*

Data were calculated for seven unique combinations of moduli and geometry. FEA were performed using models with the seven resulting hinge stiffnesses to determine the loads and displacements at each of eight profile positions across the range of motion. Figure 7 plots the maximum relative displacement at any location along any hinge versus the translational stiffness of the hinge. Curves on the figure are best-fit lines to the data from the seven hinge configurations analyzed. Figure 7 shows that the minimum stiffness parallel to the skin surface required to meet a 0.254 mm translation criterion

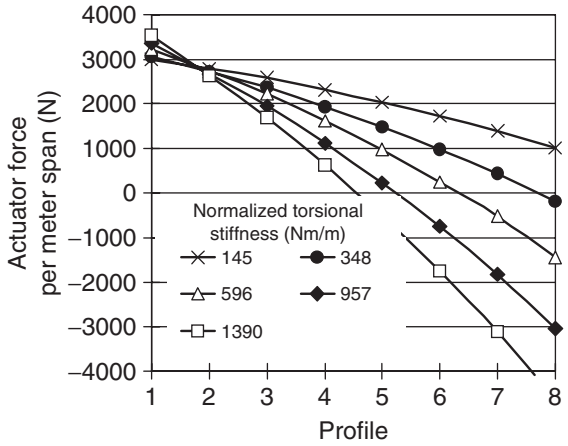

Figure 8. *Actuation force as function of hinge stiffness for lumped compliance mechanism.*

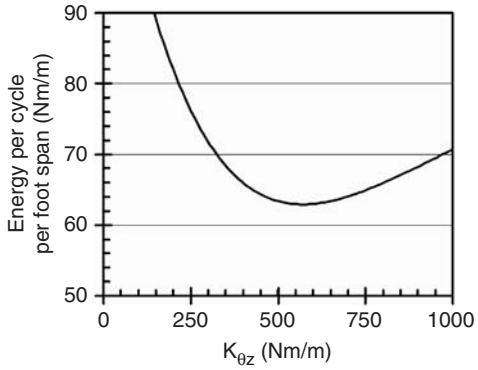

Figure 9. *Energy to move lumped compliance wing through one full cycle as function of hinge stiffness.*

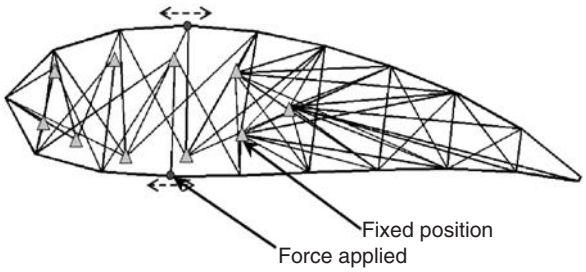

Figure 10. *Reference structure showing all possible linkage locations.*

is 1.25E8 N/m/m and that the minimum stiffness in a direction perpendicular to the skin surface is 1.09E8 N/m/m.

Actuator forces as a function of profile number are plotted in Figure 8 for five different values of torsional hinge stiffness. Stiffness values in this figure have been normalized for a unit span of wing. In Figure 8, Profile 1 is the most highly cambered (and most highly loaded by pressure) while Profile 8 is the least cambered (and has the lowest pressure loads). The actuator force shown is a combination of the force required to react external pressure and the force required to deform the hinges.

The average force between each pair of profiles was multiplied by the change in the actuator's length between each pair of profiles to approximate the work performed by the actuator. The absolute values of the calculated work for each shape were summed over the eight shapes (seven changes in position) to obtain the total work performed by the actuator per cycle:

$$W = \sum_{i=1}^{7} \left| \frac{F_i + F_{i+1}}{2} (s_{i+1} - s_i) \right| \tag{13}$$

This definition of work sums up all energy expended by the actuator when working against the spring deformation and external aerodynamic loads, and assumes that no work will be recovered during motions when the actuator is working in the same direction as the external loads. The actuator work versus the rotational stiffness is shown in Figure 9. For this system the minimum energy is achieved for a torsional hinge stiffness of 569 Nm/m. Thus, it is possible to identify appropriate values for hinge stiffness that can control the relative motion at the hinge within a prescribed tolerance while minimizing the energy expended in moving the actuator.

Design of a Distributed Compliance Mechanism

For the distributed compliance mechanism design process, it has been assumed that the skin is closed and is made of an aluminum alloy ($E = 68.9$ GPa, $\nu = 0.33$, $\sigma_y = 276$ MPa). We select the two extreme camber shapes (Positions 1 and 8 in Figure 2) as target shapes and start the design process from an intermediate profile (Position 5). Nineteen points are selected on the airfoil surface and a reference structure is created using frame elements. Locations for potential internal linkages and actuators (defined at this point as simply input forces) are shown in Figure 10. Boundary conditions in Figure 10 represent locations where the linkages would be attached to a support structure.

The actuators are placed at locations where the force can be applied nearly parallel to the motion of the skin. Two actuators locations are included in this mechanism, inside the surface of the upper and lower skins of the wing. Forces are applied at locations where the deflection of the skin in the vertical direction is a minimum over the range of motion. In the current process, intuition is used to determine where to place the actuators. Future developments will allow for the automatic identification of actuator locations that can provide actuation in an energy efficient manner.

The objective function in Equation (4) is used to maximize the efficiency and minimize the shape error. Optimization of Equation (4) has been performed using

the Method of Moving Averages (MMA) (Svanberg, 1987). The topology optimization result is shown in Figure 11. This result is one of a family of structures that result from different values of weighting functions in Equation (4). For this solution, we used weighting functions balanced toward energy minimization ($\omega_1 = 0.3$, $\omega_2 = 0.6$, $\omega_3 = 0.1$). Since the compliant mechanism has a constant perimeter length, it changes shape by the combined motion of rotation and bending of the aluminum skin rather than by in-plane stretching of the skin, which would require additional actuation force. The skin surface is a constant 3.18 mm thick. The interior sections have different thicknesses, depending on location, that range from 0.254 to 1.04 mm.

In the 2D optimization the actuators and interior legs have one end fixed in space. For an actual mechanism an internal structure is required to support the "fixed" end of the actuators and legs and to transfer load along the span of the wing and connect to the fuselage. To evaluate the effects of the use of an internal structure, a 3D FEA model has been developed and analyzed using MSC.Nastran. In the 3D model an internal wing box structure has been added without optimization to serve as this internal structure. The locations and sizing of the linkages in the model are based on the 2D topology result in Figure 11.

The FEA model is a 6.10 m wing section with clamped constraints applied to one end and a symmetry condition applied to the other end, thus representing a 12.19 m span, clamped at both ends. Ten modules, with continuous skins and 0.17 m wide legs, are spaced 0.61 m apart along the span, as shown in Figure 12. Two actuators are used for each module; one near the upper and one near the lower surface of the wing. Quasi-static aerodynamic loads were applied based on the surface pressure distributions defined from a 2D aerodynamics code. For simulating the actuation, the lengths of the actuators are prescribed and the actuation forces are recovered for static equilibrium.

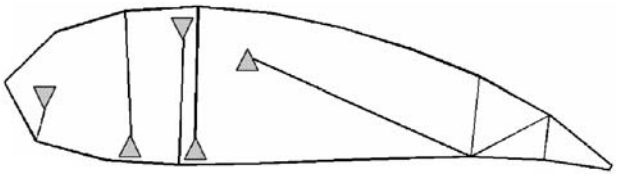

Figure 11. *Optimized topology for continuous compliant mechanism.*

Figure 13 shows views perpendicular to the leading edge of the deformed compliant wing. The figures at shown at the position of maximum camber change when actuated and are shown with and without pressure load. When actuated without pressure loading, as shown in Figure 13(a) and (b), the leading and trailing edges of the compliant wing match very closely with the target shapes, which are indicated by the open circles on each figure. The distributed compliant wing with a relatively compliant wing box is shown in Figure 13(c) and (d) under expected pressure loads.

Figure 13(c) and (d) show that the entire compliant wing deforms as the wing box bends and twists. To reduce the undesired deformation, the analysis has been performed with a very stiff wing box and the analysis results match the target shapes with minor discrepancy (Figure 13(e) and (f)). The middle top portion of the skin bulges slightly due to the surface suction, correction of which could be accomplished by thickening this portion. Stress distributions are shown in Figure 14 with both a flexible and a very stiff internal wing structure.

Actuation forces for a mechanism with and without pressure loads are shown in Table 1. Data in this table were computed using the FEA model with a stiff internal frame, and positive loads are defined as those where the actuator pushes against the structure. Without surface pressures deforming the wing to Position 1 requires more force than deforming to Position 8 because the starting profile is not exactly in the middle of the range of motion. The actuator loads are significantly different when the wing does and does not have pressure loading. In moving downward to Position 1 (from Position 5, where the skins are unstrained when no external loads are present), the actuators must work to overcome both the external aerodynamic loads and the bending of the skins. In moving upward to Position 8 the external

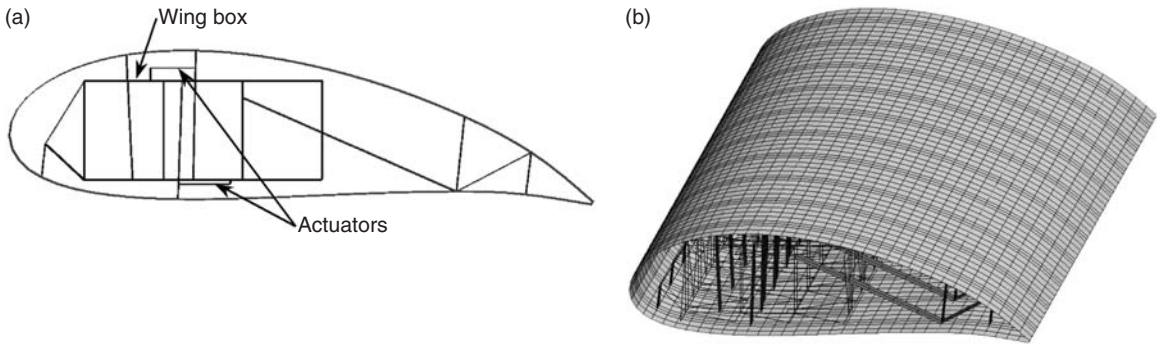

Figure 12. *FEM model of compliant wing (a) side view, (b) oblique view.*

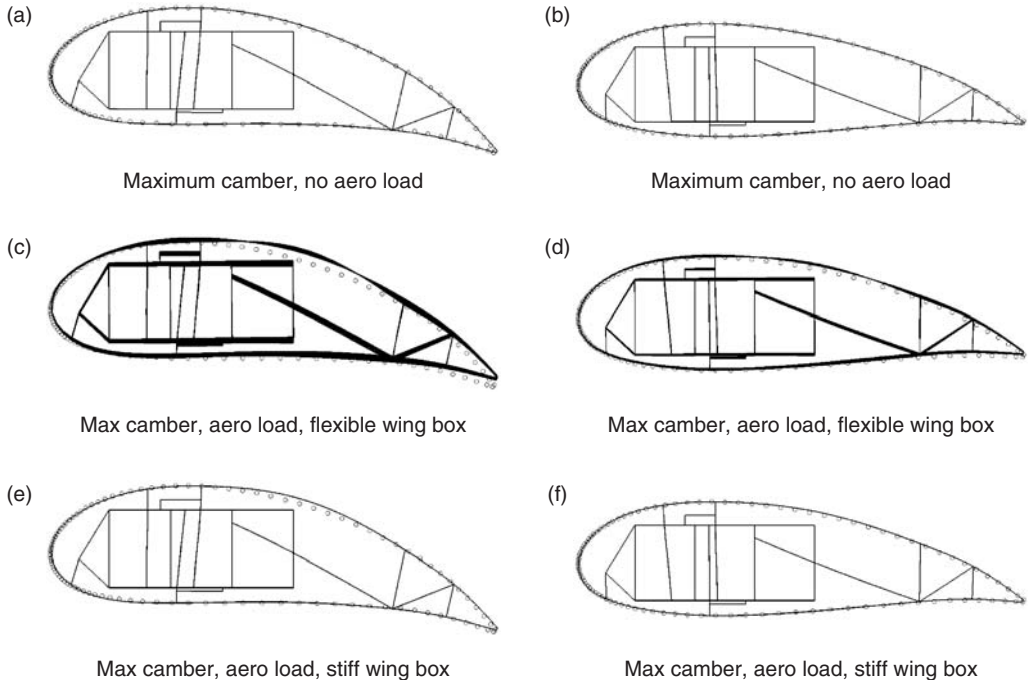

Figure 13. *Deformation of compliant wing with pressure load (viewed along wing span) (a–b) without aero loads, (c–d) with aerodynamic loads on a flexible wing box (e–f) with aerodynamic loads on a stiff wing box. Circles represent desired profiles at maximum and minimum camber positions.*

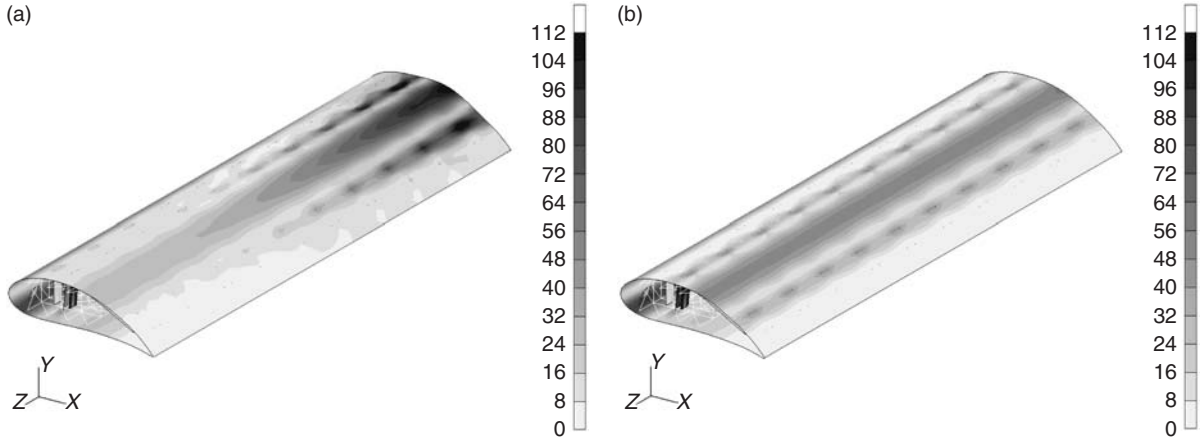

Figure 14. *Stress distribution in a compliant wing with pressure loading at minimum camber position (a) flexible wing box (b) stiffened wing box. Contours are von Mises' stress in MPa.*

Table 1. Required actuation force per module.

Target shape	Actuator location	Actuation force per module with no external aerodynamic pressure (*N*)	Actuation force per module with aerodynamic pressure applied (*N*)	Efficiency (per module)
Profile 1	Top	1378	1059	26%
	Bottom	885	3336	
Profile 8	Top	−921	−1085	113%
	Bottom	−592	640	

Table 2. Comparison of continuous and lumped compliance mechanisms.

	Continuous compliant mechanism	Lumped compliance mechanism
Exterior shape error		
RMS average (mm) at position 1	6.4	5.3
RMS average (mm) at position 8	3.3	2.8
Maximum deviation (mm) at position 1	17.8	8.9
Maximum deviation (mm) at position 8	7.9	5.6
Actuator work through cycle (Nm/m span)	143	63

aerodynamic pressures assist the actuators in deforming the wing. Defining efficiency as in Joo et al. (2003), this mechanism has an efficiency of over 100% since the pressure acting in the same direction as the wing surface movement is considered as a free energy from the air stream to help to change the shape. However, if the entire aircraft is considered as part of the control volume, the true efficiency would be <100% since some of the force required to deform the wing comes from the air stream, and can be traced originally to the fuel that is the input energy source for the entire aircraft.

Comparison of Lumped and Distributed Compliance Mechanisms

Table 2 summarizes data from the distributed and lumped compliant mechanisms generated using the FEA models. For both mechanisms the models were analyzed using a very stiff internal wing box. Table 2 shows that both mechanisms meet the desired 6.35 mm position tolerance on a root-mean-square basis, although both exceed the tolerance at the position of maximum deviation. The lumped compliant mechanism comes closer to the desired tolerance than the continuous compliant mechanism. However, the lumped compliant mechanism does have localized changes in surface contour at specific positions, whereas the continuous compliant mechanism results in a smoother surface profile.

The actuator work through one cycle was also computed for the mechanisms using the definition from Equation (13). Table 2 shows the work normalized per unit length of span. The continuous compliant mechanism requires significantly more work to move through a cycle since the actuators must supply energy to deform the skins during portions of loading when external loads are high. Lower loads and the ability to tailor hinge stiffness to minimize actuator work are one potential advantage of the lumped compliant mechanism over the continuous compliant mechanism.

SUMMARY

This article has presented design methods for developing aircraft wings with the capability to change camber using one degree of freedom mechanisms. The methods use optimization techniques to match within a desired tolerance to a set of constant arclength wing section profiles. Different design methods were developed for distributed and lumped compliance mechanisms. These design methods were applied to a representative wing section, demonstrating the feasibility of utilizing these methods for designing practical aircraft structures. The design examples concentrated on developing mechanisms that utilize an internal wing box for load transfer along the length of the wing, which may result in a heavy wing.

ACKNOWLEDGMENT

The authors would like to thank Kristen Svanberg of Sweden's Royal Institute of Technology for providing the code used for performing the optimization using the method of moving asymptotes. We would also like to thank Jason Bowman of the Air Force Research Laboratory for developing the optimal wing sections used in the applications section of this article.

REFERENCES

Ananthasuresh, G.K. and Kota, S. 1995. "Designing Compliant Mechanisms," *ASME Mechanical Engineering*, November, 117(11):93–96.

Arun, K.S., Huang, T.S. and Blostein, S.D. 1987. "Least-squares Fitting of Two 3-D Point Sets," *IEEE Transactions on Pattern Analysis and Machine Intelligence*, PAMI-9(5):698–700.

Hall, J.M. 1989. "Executive Summary AFTI/F-111 Mission Adaptive Wing," WRDC-TR-89-2083, September.

Horn, B.K.P. 1987. "Closed-form Solution of Absolute Orientation using Orthonormal Matrices," *Journal of the Optical Society of America*, 5(7):1127–1135.

Horn, B.K.P. 1987. "Closed-form Solution of Absolute Orientation using Unit Quaternions," *Journal of the Optical Society of America*, 4(4):629–642.

Joo, J., Kota, S. and Kikuchi, N. 2000. "Topological Synthesis of Compliant Mechanisms Using Linear Beam Elements," *Mechanics of Structures and Machines*, 28(4):245–280.

Joo, J. 2001. *Synthesis of Compliant Mechanisms: Topology and Size and Shape Design*, PhD Dissertation, Department of Mechanical Engineering, University of Michigan, Ann Arbor.

Joo, J., et al. 2003. "Energy Based Efficiency of Mechanized Solid-State Actuators," *SPIE Smart Structures and Materials Conference*, March 2–6, San Diego, California.

Korte, B.M., Murray, A.P. and Schmiedeler, J.P. 2006. "Synthesis of Planar, Shape-Changing Rigid-Body Mechanisms," In: *Proceedings of the 2006 ASME International Design Engineering Technical Conferences & Computers and Information in Engineering Conference*, September 10–13, Philadelphia, Pennsylvania.

Kudva, J.N. 2004. "Overview of the DARPA/AFRL/NASA Smart Wing Project," *Journal of Intelligent Material Systems and Structures*, 15(4):261–267.

Reich, G.W., Bowman, J.B. and Sanders, B. 2004. "Large Area Control for Aerodynamic Control of Long Endurance Sensor Platforms," in publication in *Journal of Aircraft*.

Sigmund, O. 1997. "On the Design of Compliant Mechanisms Using Topology Optimization," *Mechanics of Structures and Machines*, 25(4):493–524.

Skelton, R.E. 2001. "An Introduction to the Mechanics of Tensegrity Structures," from http://www.mae.ucsd.edu/research/reskelton/

Svanberg, K. 1987. "The Method of Moving Asymptotes – A New Method for Structural Optimization," *International Journal for Numerical Methods in Engineering*, 24:359–373.

Umeyama, S. 1991. "Least-squares Estimation of Transformation Paramaters between Two Point Patterns," *IEEE Transactions on Pattern Analysis and Machine Intelligence*, 13(4):376–380.